PHYSICS

Coherent electric field manipulation of Fe^{3+} spins in $PbTiO_3$

Junjie Liu[1]*, Valentin V. Laguta[2]*, Katherine Inzani[3,4]*, Weichuan Huang[5], Sujit Das[5,6], Ruchira Chatterjee[7], Evan Sheridan[3,4], Sinéad M. Griffin[3,4], Arzhang Ardavan[1†], Ramamoorthy Ramesh[3,5,6†]

Magnetoelectrics, materials that exhibit coupling between magnetic and electric degrees of freedom, not only offer a rich environment for studying the fundamental materials physics of spin-charge coupling but also present opportunities for future information technology paradigms. We present results of electric field manipulation of spins in a ferroelectric medium using dilute ferric ion–doped lead titanate as a model system. Combining first-principles calculations and electron paramagnetic resonance (EPR), we show that the ferric ion spins are preferentially aligned perpendicular to the ferroelectric polar axis, which we can manipulate using an electric field. We also demonstrate coherent control of the phase of spin superpositions by applying electric field pulses during time-resolved EPR measurements. Our results suggest a new pathway toward the manipulation of spins for quantum and classical spintronics.

INTRODUCTION

Manipulation of magnetism by an electric field instead of a magnetic field is driving substantial research activity in condensed matter physics, motivated not only by the intriguing fundamental materials physics but also by the potential applications in future low-power spintronics (*1*–*8*). On the basis of insulating multiferroic heterostructures, one is able to switch the magnetization by an electric field rather than electric current, thus providing a pathway to significantly reduce energy consumption (*1*). In the past decade, numerous pathways for electric field control of magnetism have been envisaged, and several interesting physical mechanisms have also been revealed, including interfacial strain/stress coupling (*9*, *10*), charge mediation (*11*–*13*), exchange bias or coupling at ferromagnetic-antiferromagnetic interfaces (*14*–*17*), manipulation of state of 3d orbitals (*18*, *19*), etc.

However, all these approaches are mainly focused on the manipulation of the magnetization in materials with macroscopic long-range magnetic order (i.e., ferro/ferri/antiferromagnets). As a step toward understanding the fundamental limits of these magnetoelectric coupling phenomena, one could ask the question: Is it possible to manipulate isolated spins, as opposed to long-range ordered states, using an electric field? In addition to presenting an intriguing fundamental science challenge with the potential to affect quantum computing, it would be valuable to manipulate spin-spin interactions and the spins of individual atoms or ions (*20*). Recently, electric field control of individual molecular magnets and tuning of magnetic exchange in a molecular system were achieved (*21*–*23*). These results show the fascinating potential for spin-electric coupling (*24*), which belongs to the family of magnetoelectric effects.

Complex oxides that include transition metal or rare earth ions can have charge, spin, orbital, and lattice degrees of freedom that interact and give high tunability at a microscopic level for desirable macroscopic properties. For example, the strong polarization and lattice control in perovskite oxides have enabled the strain coupling of ferroelectricity and multiferroic orders, which is generating emerging logic and storage approaches (*1*). The role of aliovalent cationic impurities, such as Fe^{3+} in $PbTiO_3$, has been studied extensively from the perspective of how the impurities interact with ferroelectric domain walls and, thus, influence the switching and degradation mechanisms (*25*, *26*). In particular, electron paramagnetic resonance (EPR) has been extensively used to probe the electronic structure of these impurities. However, there has been no work focused on understanding the spin state and manipulating the spins in these impurities using an electric field.

With this as the background, we demonstrate coherent electric field manipulation of spins doped into a prototypical ferroelectric, $PbTiO_3$ in which Fe^{3+} (high spin $S = 5/2$, $3d^5$ electronic structure) is inserted into the Ti^{4+} site (*27*, *28*). We found that the spins in the Fe^{3+} ions are oriented normal to the dz^2 orbital direction as a consequence of spin-orbit coupling within the Fe^{3+} ion, while the orbitals are coupled to the tetragonal polar lattice distortion that is characteristic of this ferroelectric. We demonstrate through both ab initio calculations and EPR-based experiments that the spins can be switched in a nonvolatile fashion and coherently manipulated with an electric field applied to the ferroelectric layer. The results described in this work are representative of a large class of materials in which the polar order and the accompanying coupling to the spins can be systematically tuned and manipulated, thus opening a new door to explore pathways for full electric field control of spins in individual ions. Although our work is focused on exploring the limits of magnetoelectric coupling down to single ions, this work has possible implications for potential quantum computing and spintronics applications.

RESULTS

Ab initio calculations were performed within the density functional theory (DFT) framework to get insight into the interaction between electric polarization and spin behavior. Fe^{3+} doping was modeled

[1]CAESR, Department of Physics, University of Oxford, The Clarendon Laboratory, Parks Road, Oxford OX1 3PU, UK. [2]Institute of Physics of the Czech Academy of Sciences, Cukrovarnická 10, 162 00 Prague, Czech Republic. [3]Materials Sciences Division, Lawrence Berkeley National Laboratory, Berkeley, CA 94720, USA. [4]Molecular Foundry, Lawrence Berkeley National Laboratory, Berkeley, CA 94720, USA. [5]Department of Materials Science and Engineering, University of California, Berkeley, CA 94720, USA. [6]Department of Physics, University of California, Berkeley, CA 94720, USA. [7]Molecular Biophysics and Integrated Bioimaging Division, Lawrence Berkeley National Laboratory, Berkeley, CA 94720, USA.
*These authors contributed equally to this work.
†Corresponding author. Email: arzhang.ardavan@physics.ox.ac.uk (A.A.); rramesh@berkeley.edu (R.R.)

with 1 Ti^{4+} of 27 replaced by Fe^{3+} (details of the calculations are provided in Materials and Methods). The spin axis was varied relative to the ferroelectric dipole as depicted in Fig. 1A, allowing a comparison of energies for different spin directions. We considered two cases: first, a direct replacement of a Ti^{4+} with a Fe^{3+} and, second, a representative Fe-O defect complex to account for the valence difference. For the first case, we find that in the polar state with the tetragonal lattice distortion in the [001] direction, the lowest-energy spin direction is perpendicular to the ferroelectric dipole. The easy plane is perpendicular to the tetragonal distortion, with a calculated magnetocrystalline anisotropy energy (MCAE) of 530 μeV between the parallel and perpendicular directions, in reasonable agreement with the experimental value of 720 μeV (extracted from EPR measurements; see below). Varying the spin axis within the (001) plane gives an energy difference of only 5 μeV between the [100] and [110] directions, thus resulting in a spin easy plane. The presence of the Fe_{Ti}/O-vacancy defect complex reduces the MCAE to ~300 μeV, but the spin easy plane remains in the plane perpendicular to the ferroelectric dipole (Fig. 1B).

We then studied the influence of ferroelectric dipole rotation (through the application of an electric field) on the magnetic anisotropy. In the nonpolar, cubic structure, the spin axis was degenerate as it was varied in the (001) plane (Fig. 1B). In this case, the high-spin Fe $3d^5$ orbital momentum is quenched in the O_h crystal field, resulting in no preferred spin axis. With a tensile strain along the *c* axis to vary the magnitude of the ferroelectric dipole, the displacement of Fe along the *c* axis results in a spin easy plane in the *ab* plane. This ferroelectric distortion breaks the parity symmetry of orbitals orthogonal to this displacement, inducing an orbital moment and results in a spin easy plane perpendicular to the ferroelectric distortion. Although there is C_4 rotational symmetry around the polar axis, the charge density (shown in fig. S1A) is rather isotropic, resulting in effectively degenerate and isotropic spin axes in-plane. Therefore, we find that the MCAE is proportional to the tetragonality as shown in Fig. 1C. In switching the ferroelectric dipole from [001] to [010], the structure passes through an intermediate monoclinic phase in which the dipole aligns along the [011] direction (as described in the Materials and Methods). This intermediate monoclinic structure has an MCAE of 164 μeV with a spin easy axis along the [100] direction, confirming that the spin direction still remains perpendicular to the ferroelectric dipole. Thus, we conclude that the combination of spin-orbit coupling and the distorted crystal field provided by the symmetry-breaking ferroelectric displacement determines the magnetocrystalline anisotropy.

We performed experiments on weakly Fe^{3+}-doped [20 to 50 parts per million (ppm)] $PbTiO_3$ single crystals using EPR spectroscopy as shown in Fig. 2. A typical EPR spectrum is shown in Fig. 2A (right); the magnetic field is applied parallel to [100], i.e., perpendicular to the *c* axis. A single strong line is visible, and there are several weaker subsidiary lines. We can assign these to transitions between m_S states within the $S = 5/2$ multiplet, where m_S represents good quantum numbers for a magnetic field applied along the *c* axis. The strong line corresponds to the $-1/2 \leftrightarrow 1/2$ transition; a somewhat

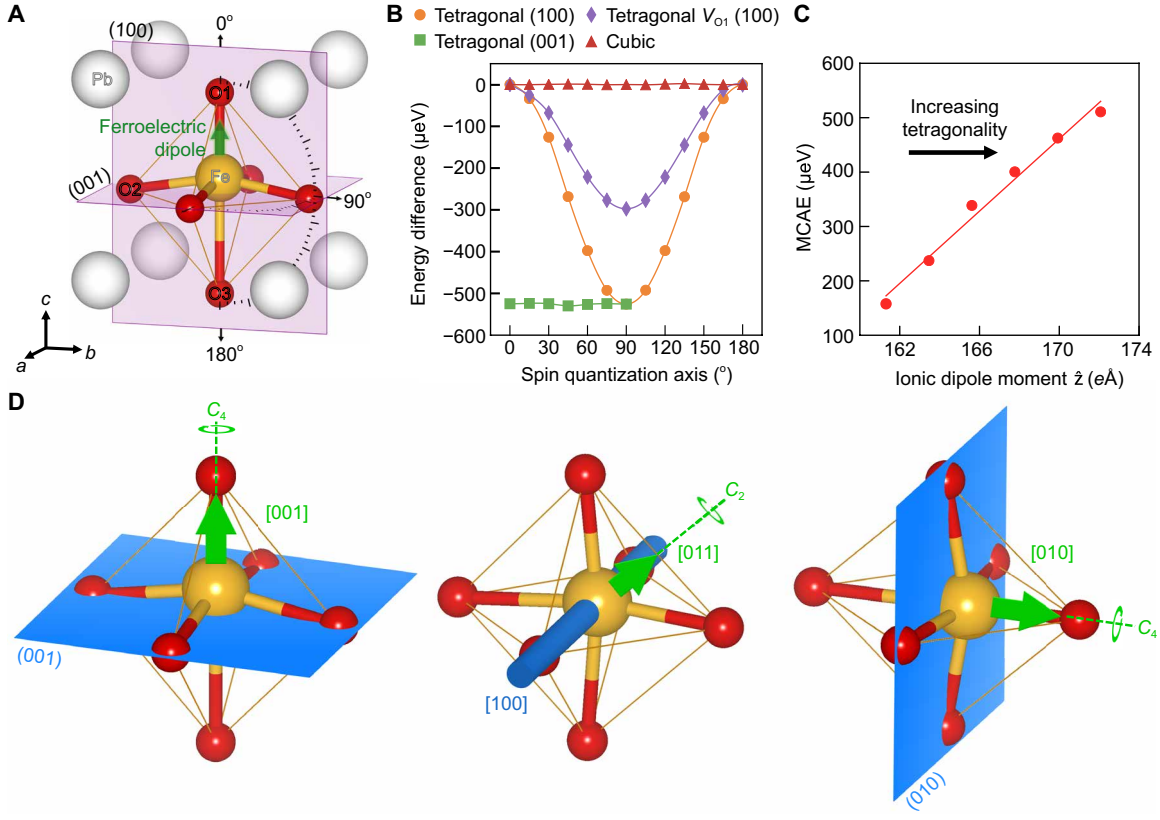

Fig. 1. Ab initio theoretical calculations demonstrating magnetic anisotropy dependence on ferroelectricity. (**A**) Schematic showing the angle of the spin axis relative to the ferroelectric dipole [001], varied within the (100) and (001) planes. (**B**) Difference in total energy as the spin axis is varied within the tetragonal structure, cubic structure, and tetragonal structure with an oxygen vacancy on the O1 site (V_{O1}). (**C**) MCAE with change in ionic dipole moment in strained tetragonal structure. (**D**) Schematic of the spin easy plane or easy axis (blue) with change in ferroelectric dipole (green) and rotational symmetry about the polar axis.

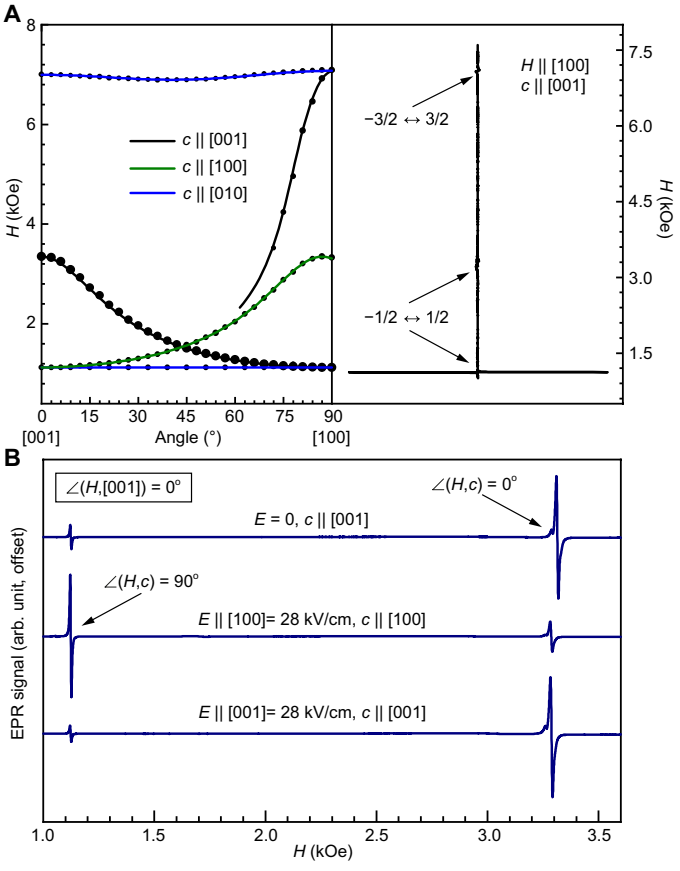

Fig. 2. Electric field manipulation of the ferroelectric order in $PbTiO_3$ crystals, detected through continuous-wave EPR of Fe^{3+} dopant spins. (**A**) Left: Angular dependence of the X-band (9.4 GHz) Fe^{3+} resonance fields measured at 296 K. Dots indicate the magnetic field positions of resonances as a function of magnetic field orientation; the dot size indicates the intensity of the corresponding transition. Solid lines are calculated data. Right: A typical EPR spectrum, from which the resonance positions and intensities are extracted. (**B**) A sequence of EPR spectra for a magnetic field applied along [001], for a pristine sample (upper trace), following reconfiguration of the ferroelectric order by application an electric field along [100] (middle trace), and following restoration of the original ferroelectric order by application of an electric field along [001]. arb. unit, arbitrary units.

weaker line corresponds to the −3/2 ↔ 3/2 "forbidden" transition. We assign the observed spectrum to isolated Fe^{3+} ions, which replace Ti^{4+} ions with charge compensation far away from the paramagnetic ion. This is based on the fact that the tetragonal crystal field constant of this ion approaches zero when the temperature increases to the cubic-tetragonal phase transition, i.e., it follows well the c/a-1 ratio (*27*). In contrast, the Fe_{Ti}/O-vacancy center, which may also occur in $PbTiO_3$:Fe (*28*), exhibits a tetragonal constant that is much less sensitive to temperature as the vacancy creates a strong tetragonal distortion in vicinity of a paramagnetic ion, even in the cubic phase (*29*).

The large tetragonal crystal field of the $PbTiO_3$ lattice (*27*, *28*) mixes states within the $S = 5/2$ multiplet when the magnetic field deviates from the tetragonal axis, so the states involved in the transitions are not pure $m_S = \pm 1/2$ and $\pm 3/2$. This, in turn, leads to a strong dependence of the magnetic field position of the resonances as a function of the orientation of the magnetic field with respect to the crystal axes. This is demonstrated by the angular dependences of the resonance fields measured under rotation of the magnetic field, H, from the [001] to the [100] direction (Fig. 2A, left).

The effective g factor for the −1/2 ↔ 1/2 transition varies between $g_{eff} = 5.970$ for $H \perp c$ (angle $\theta = 90°$, corresponding to an EPR transition at $H_{res} = 1123$ Oe) and $g = 2.0056$ ($H_{res} = 3342.5$ Oe) for $H // c$ (angle $\theta = 0°$). Thus, the H-field position of the EPR transition offers us a probe of the local orientation of the ferroelectric polarization; conversely, by manipulating the ferroelectric polarization, we have control over the Fe^{3+} spin Hamiltonian. In particular, the strongest line in the Fe^{3+} spectrum corresponds to spins located in the domains with c // [001]. The other two lines (two orders weaker in intensity: blue and green lines in Fig. 2A, left) arise from spins in 90° domains with c axes in the (001) plane (i.e., a minority fraction of 90° domains in the crystal).

The angle dependence of the EPR spectra allows us to experimentally determine the spin anisotropy, as parameterized by the Hamiltonian (Eq. 1 in Materials and Methods) whose dominant anisotropy term is of the form $-DS_z^2$. The solid lines in Fig. 2A (left) are fits to the data yielding $D = 120$ μeV, i.e., an easy plane. This corresponds to a zero–magnetic field splitting between the $m_S = \pm 5/2$ and $m_S = \pm 1/2$ doublets of 720 μeV, which corresponds favorably with the calculations of the MCAE reported above.

This anisotropy experienced by the spins is imposed by the local ferroelectric order. It allows us to control the anisotropy axis by manipulating the ferroelectric polarization direction via application of an external electric field that exceeds the coercive field for 90° ferroelastic switching. We demonstrate this (see Fig. 2B) by recording a sequence of EPR spectra with the magnetic field parallel to [001]. The upper trace is for the pristine sample for which the c axis is along [001]. The middle trace shows the spectrum following application of an electric field of 28 kV/cm along [100] to switch the c axis perpendicular to the magnetic field. The process is fully controllable, as demonstrated by the lower trace, which follows application of the electric field of 28 kV/cm along [001] to restore the original electric polarization axis. The electric polarization in each state is stable in time, so this process amounts to nonvolatile controlled configuration of the spin Hamiltonian using an electric field.

Note that, here, we used weakly Fe-doped crystals in which the Fe^{3+} spins may be considered as isolated noninteracting spins under the experimental conditions we studied. For a given concentration of Fe, spin-spin interactions (predominantly dipolar for low concentrations and with an exchange contribution at sufficiently high concentrations) with an energy scale J will give rise to spin correlations below temperatures of order J/k_B (where k_B is the Boltzmann's constant), which is in the microkelvin range for the samples we study here. We expect any such correlations to be sensitive to the ferroelectric order.

To determine the transverse spin relaxation (or phase memory) time T_2, we performed EPR spin echo measurements (details in Materials and Methods and fig. S2) on the single crystal sample. Figure 3A shows spin coherence times as a function of temperature for several of the electron spin resonance transitions. These are derived from exponential fits, $A_{echo}(\tau) \propto \exp.(-2\tau/T_2)$ to the Hahn echo decays. A typical Hahn echo decay is shown in the inset, demonstrating a simple exponential dependence of the echo amplitude on the delay time τ; the fast modulations of the echo arise from the interaction of Fe^{3+} spins with ^{207}Pb and $^{47,49}Ti$ nuclear spins [electron spin echo envelope modulation (ESEEM)].

When H is parallel to the c axis, the π/2 microwave pulse generates a coherence between ±1/2 states whose energy separation is determined

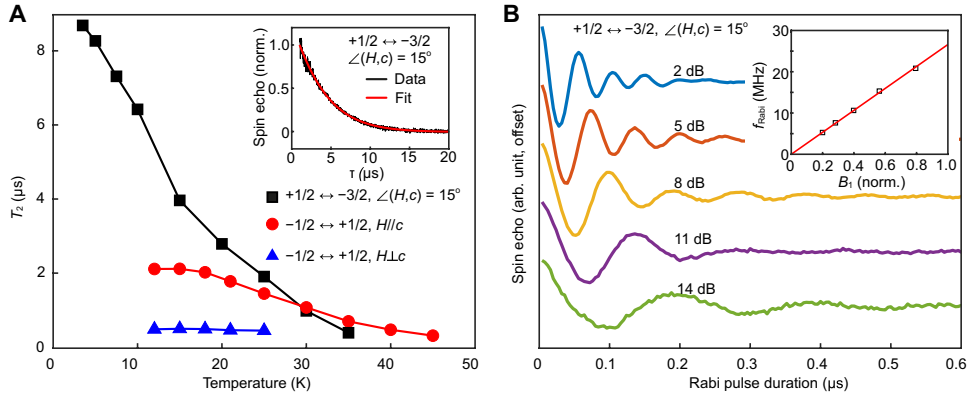

Fig. 3. Spin coherence and Rabi oscillations. (**A**) Temperature dependence of the spin coherence (spin memory) time T_2 for both $H//c$ and $H\perp c$. The details for the EPR transitions can be found in fig. S2. The inset is the spin echo signal amplitude as function of echo delay time for +1/2 ↔ −3/2 B transition (recorded with H tilted 15° from c axis) in $PbTiO_3$ crystal at 3.5 K, where the T_2 is about 8.7 μs. (**B**) Echo intensity versus the duration of the Rabi pulse at different pulse powers. The inset shows the linear correlation between the Rabi frequency f_{Rabi} and the microwave B_1 field (normalized against the B_1 field without any attenuation).

almost entirely by g_z and the phase memory time is as long as 2 μs at 12 K. However, when the magnetic field is oriented perpendicular to the c axis and the anisotropy terms in the spin Hamiltonian mix states within the S = 5/2 multiplet, the transition energy depends also on these anisotropy energies. Fluctuations in these terms will contribute to phase relaxation, explaining why the phase memory time is significantly shorter for this H-field orientation. Overall, the coherence time in our system (reaching ~9 μs for the high-field, +1/2 ↔ −3/2 transition at low temperatures) is of the same order of magnitude as some of the currently proposed spin qubits (*30*, *31*). The anisotropy in T_2 illustrates that the fluctuations driving phase relaxation are also highly dependent on H-field orientation. The presence of ESEEM in the echo decay indicates that the magnetic nuclei ^{207}Pb and ^{47,49}Ti may also be involved in the phase relaxation and that the coherence is likely to be enhanced by isotopic purification of the $PbTiO_3$. Figure 3B shows Rabi oscillations, demonstrating that coherent manipulation of these spin states can be achieved via microwave pulse control.

The fact that the spin-bearing Fe^{3+} ions lie in an environment that lacks inversion symmetry provides an alternative means of coherently controlling the quantum spin states via the linear electric field effect (*32*). We investigate this interaction by inserting an electric field pulse into a standard Hahn echo EPR sequence (Fig. 4B and fig. S3). The effect for $E//c$ axis is shown in Fig. 4C. The low-field −1/2 ↔ +1/2 transition (*32*) shows little modification with the application of an electric field because it only weakly depends on crystal field modification. By contrast, a pronounced modulation of the spin echo transient is observed for the high-field +1/2 ↔ −3/2 transition (Fig. 4A) when the electric field pulse is applied. The integrated in-phase echo shows a cosine-shaped oscillation pattern superimposed onto a quasi-exponential decay as t_E increases from zero to $t_E = \tau$ (i.e., 4 μs), while the quadrature component of the echo exhibits a sine dependence on t_E, also overlaid onto a quasi-exponential decay. This oscillation is due to an E field–induced change in the EPR resonance frequency via electric field modulation of the axial magnetocrystalline anisotropy, leading to a phase shift in the echo signal (*32*, *33*). The decay in the echo amplitude is due to the inhomogeneity in the electric field across the crystal, resulting from the irregularity crystal shape and the high relative permittivity for $PbTiO_3$. The echo subsequently recovers to its original value when $t_E = 2\tau$ (i.e., 8 μs), as the phase shift induced by the electric field during the first period of free evolution (between the π/2 and π pulses) is reversed by the π pulse and progressively canceled. This confirms that the interaction between the spins and the electric field is coherent.

DISCUSSION

A linear dependence of the spin echo intensity on the electric field is expected because of the lack of inversion symmetry in the local coordination environment for Fe^{3+}. This is confirmed in Fig. 4D, which shows a linear dependence of the change in the EPR resonance frequency and the amplitude of the applied electric field. Furthermore, the difference between the −1/2 ↔ +1/2 and +1/2 ↔ −3/2 transitions indicates that the axial anisotropy parameter, D, is sensitive to the applied E field, while the Lande g factor is insensitive to this stimulus. This is further confirmed by measuring the electric field effect for the 1/2 ↔ −3/2 and −3/2 ↔ +3/2 ($H \perp c$) transitions (fig. S4). A similar dependence has been reported for Mn^{2+} in ZnO (*33*). However, note that using a ferroelectric as the host medium, the spin-electric coupling coefficient is three times larger than that of ZnO:Mn^{2+} and significantly larger than for paramagnetic dopants in silicon (see Materials and Methods and fig. S5) (*34*). The ferroelectric medium provides a mechanism for dynamically configuring the anisotropy for a given spin using local electrostatic gates. This raises the possibility of a field-programmable gate array, in which an array of bits can be dynamically configured in the hardware (schematically proposed in fig. S6). There are proposed quantum computing schemes that exploit heterogeneous qubits (*35*, *36*); magnetic defects in ferroelectric hosts could offer a physical context in which these ideas may be explored. Our experimental observations may stimulate theoretical developments leveraging the spin configurability that we have demonstrated.

In summary, we present the first observations of electric field–dependent magnetocrystalline anisotropy and coherent spin manipulation in ferroelectric Fe-doped $PbTiO_3$. EPR spin echo measurements reveal spin coherence lifetime of the order of a few microseconds. We believe that this can be significantly enhanced by appropriate design of the ferroelectric material (e.g., its tetragonality, the chemical species, isotopic purity, etc.). More broadly, a wide spectrum of

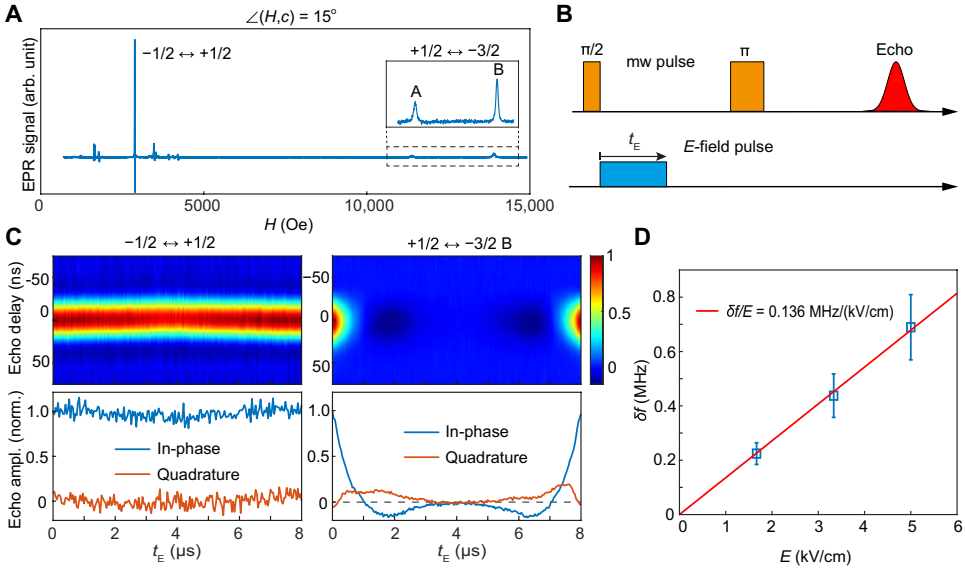

Fig. 4. Coherent electric field spin control in Fe-$PbTiO_3$ crystals. (**A**) The continuous-wave EPR signal in $PbTiO_3$ crystal with *H* applied 15° away from the *c* axis. The EPR transitions for Fe^{3+} are labeled as −1/2 ↔ +1/2 and +1/2 ↔ −3/2 A and B (see fig. S2 for more details). (**B**) Schematic of the *E*-field experimental pulse sequence. A standard Hahn echo microwave (mw) sequence is used to measure the spin echo signal. A DC electric field pulse is applied immediately after the π/2 pulse. The echo signal is recorded as function of the electric pulse duration (t_E). (**C**) The transient in-phase echo (top) and integrated echo intensity (bottom) as a function of t_E for the −1/2 ↔ +1/2 and +1/2 ↔ −3/2 B resonances with the applied voltage of 1.67 kV/cm. The *E* field is applied parallel to the *c* axis. The separation between the π/2 and π pulses, τ, is fixed to 4 μs, while t_E is varied from 0 to 2τ. (**D**) The change in the EPR transition as a function of the applied electric field.

ferroelectric materials, spanning inorganic oxides to polymeric systems such as polyvinylidene fluoride (*37*), presents an attractive platform to explore electric field control of magnetic properties for quantum or classical spintronics applications.

MATERIALS AND METHODS

DFT calculations

DFT calculations were carried out on 3 × 3 × 3 supercells of $PbTiO_3$ (135 atoms) including one Fe ion on a Ti site with one electron added to correctly compensate the Fe^{3+} charge state ($Fe_{Ti}^{'}$). The Fe-Fe distance of 11.625 Å ensured that the dopant ions were sufficiently isolated from each other. The Fe ion/O-vacancy defect complex was considered with a doubly ionized vacancy ($V_O^{\cdot\cdot}$) on the site of the apical oxygen with the shortest Fe—O bond length. The Vienna Ab initio Simulation Package (*38*–*40*) was used with projector augmented wave pseudo-potentials (*41*, *42*) including Pb d,s,p; Ti s,p,d; Fe d,s; and O s,p electrons as valence. A plane wave cutoff energy of 750 eV was used with a 2 × 2 × 2 Gamma-centered *k*-point grid, which converged the total energy to 1 meV per formula unit. The PBEsol functional was used which gave $PbTiO_3$ lattice parameters within 1% of experimental values. Atomic positions were relaxed within spin-polarized calculations until the residual forces on each atom were less than 0.01 eV/Å. For optimization of the doped structure with tetragonal ferroelectric displacement, the volume and cell shape were held fixed to those of undoped $PbTiO_3$, while for the cubic structure, the symmetry was also constrained. To generate the monoclinic structure, starting from the $PbTiO_3$ cubic unit cell, Ti was displaced along the [011] direction, and the ion positions, cell volume and shape were allowed to relax within symmetry constraints until the forces on each atom were less than 0.001 eV/Å. From this structure, a 3 × 3 × 3 supercell was constructed, and 1 Ti of 27 was replaced with an Fe ion. The ionic positions were again optimized with the dopant present to a force convergence of 0.02 eV/Å, with symmetry constrained and supercell volume and shape fixed.

The magnetocrystalline anisotropy was calculated by including spin-orbit coupling self consistently and varying the spin quantization axes. An effective Hubbard term $U_{eff} = U - J = 4$ eV was added to the Fe d orbitals within the Dudarev approach (*43*). The effect of the exchange-correction (*J*) parameter was tested for *J* = 0 to 1.8 eV with *U* = 4 eV and was found to increase the MCAE (fig. S1) but did not change the spin easy axis and thus did not affect the magnetic ground state.

Sample preparation

The $PbTiO_3$ single crystal used in pulsed EPR measurements was grown by a flux method using the B_2O_3-PbO melt containing stoichiometric amounts of $PbCO_3$ and TiO_2. The crystal had a majority of 180° domains oriented parallel to the crystal *c* axis perpendicular to the main face, and the content of 90° domains was less than 1%. Fe^{3+} was present in the crystal as accidental impurity at a concentration of 20 to 50 ppm. The Fe^{3+} concentration was estimated from Fe^{3+} EPR intensity in the usual way by comparing the EPR intensity in our crystals with the EPR intensity of Cr^{3+} in a MgO reference sample with known concentration of Cr^{3+}. The typical crystal size in measurements was about 2 mm by 3 mm by 0.35 mm. For experiments with 90° switching of the polarization, the crystal dimensions were 1.2 mm by 0.7 mm by 0.5 mm, with the surfaces parallel to crystallographic (100) planes. To apply electric fields at two perpendicular directions, [100] and [001], electrodes were applied to the corresponding crystal surfaces using flexible silver paste (SPI-paint). The crystal with electrodes was also electrically insulated by picein compound, allowing application of electric fields up to 30 kV/cm.

EPR analysis

The EPR spectra for $PbTiO_3$ single crystal were carried out using Bruker E580 spectrometer. The following spectrometer parameters were used: a microwave frequency of 9.34 to 9.44 GHz, a temperature range of 3.5 to 296 K, a field modulation amplitude of 1.5 G at 100 kHz, and a microwave power of 0.2 mW. Pulsed EPR measurements to obtain spin memory time were also carried out using a Bruker E580 spectrometer and standard Bruker MD5 resonator with the resonance frequency of 9.75 GHz. Spin echo decay as a function of the pulse separation τ between π/2 and π microwave pulses was recorded in the Hahn echo pulse sequence π/2-τ-π-τ-echo (*44*). The length of π/2 pulse was 16 ns and τ varied from 200 to 20,000 ns with an increment of 4 ns.

EPR spectra were interpreted using spin Hamiltonian of the general form for Fe^{3+} ion ($3d^5$, $S = 5/2$) in the tetragonal symmetry

$$\mathbf{H} = \frac{1}{3}DO_2^0 + \frac{1}{180}FO_4^0 + \frac{1}{120}a(O_4^0 + 5O_4^4) + G_zH_zS_z + G_xH_xS_x + G_yH_yS_y \quad (1)$$

with $G_i = \beta g_i$ and the usual definitions of the O_l^m operators. Here, D and F parameters correspond to axial (tetragonal) crystal fields of the second and fourth degree, respectively, with the z axis chosen along the direction of the axial crystal field, i.e., along the tetragonal c axis. a is the cubic crystal field splitting parameter. The zero-field splitting parameters determined for bulk crystal at both the room temperature ($T = 296$ K) and low temperatures ($T < 20$ K). At the room temperature, $D = 0.9650\ cm^{-1}$, $a = 0.01\ cm^{-1}$, and $F = -0.0108\ cm^{-1}$. Below 20 K, $D = 1.18\ cm^{-1}$, $a = 0.056\ cm^{-1}$, and $F = -0.094\ cm^{-1}$. The g factor is almost isotropic: $g_z = 2.0056$ and $g_{x,y} = 2.009$. The temperature dependences of the zero-field splitting parameters are consistent with those reported in (*27*, *28*).

Electric field dependent EPR analysis

The zero-field splitting of the Fe^{3+} energy levels, i.e., the parameter D in Eq. 1, can also depend on the external electric field, as we have shown by direct measurement of electric field influence on the zero-field splitting parameter. Measurements were performed for $PbTiO_3$ crystal with c domain structure at different temperatures by applying an electric field parallel to the c axis. The magnetic field H was applied in two directions: (i) 15° away from the c axis to measure the spectral line of the high-field +1/2↔ −3/2 transitions (Fig. 4A) and (ii) perpendicular to the c axis to measure the −3/2↔ +3/2 transition (fig. S4C). All these transitions are sensitive to small modifications in the D parameter (fig. S2, E and F). For example, fig. S5 shows the EPR line under the application of an electric field in the range +30.3 to −24.2 kV/cm. The spectral lines linearly shift in the electric field. Note that value of the negative electric field was restricted to −24 kV/cm as at higher fields the electric polarization starts to switch to the opposite direction, leading to a reverse of the EPR line shift as well. Using the data of fig. S5, the spin-electric coupling coefficient was calculated from the relation: $D(E) = D(E = 0) + \kappa E$, where $\kappa = 10\ Hz\ V^{-1}\ m$ and $D(E = 0) = 32.740$ GHz. This is a relatively large value, compared, for instance, with the equivalent parameter in $ZnO:Mn^{2+}$, which is three times smaller (*33*). We note that the spin-electric coupling observed in Fig. 4 ($\kappa = 1.7\ Hz\ V^{-1}\ m$) is weaker than this by a factor of approximately 6. This is because, in the experiment reported in Fig. 4, the electrodes applying the electric field pulses were insulated from the $PbTiO_3$ crystal; in this configuration, because of the large relative permittivity, which for $PbTiO_3$ is $\varepsilon_r \approx 50$ (*45*), the electric field leads to a polarization surface charge that significantly screens the field in the bulk. In addition, this, combined with the unevenness in the thickness of the crystal, caused the inhomogeneity in the electric field and the rapid decay in the echo signal shown in Fig. 4C. In contrast, the data in fig. S5 were obtained with the electrodes in direct contact with the $PbTiO_3$ crystal surface, thus suppressing the screening effect of the surface charge.

Comparison with other solid-state quantum systems

The coherent spin-electric field coupling raises the possibility of quantum spin control with electric fields in $PbTiO_3$. Here, we discuss the electric field required for nontrivial spin operations using both the nonresonant (*7*) and resonant (*2*) approaches.

We first consider the nonresonant approach for local spins control. Kane proposed an A-gate (*7*) in which a local electric field is applied to shift the resonance frequency of a spin out of/into the band width of a global microwave radiation pulse, hence achieving selective manipulation for identical spin qubits. We consider this approach for the −3/2 ↔ +3/2 transition of Fe^{3+} in $PbTiO_3$ with the magnetic field applied perpendicular c axis. The electric field measurement (fig. S5A) shows that the transition frequency, f_{34}, is tuned by the externally applied field such that $\delta f_{34}/E = 4\ Hz\ V^{-1}\ m$, where $\delta f_{34} = \delta f_{34}(E) - \delta f_{34}(E = 0)$ is the change in the EPR frequency. For a microwave pulse of 100 ns (~ $T_2/100$), a DC electric field of 25 kV/cm is sufficient to tune the spin on/off resonance with the global microwave radiation. Such an electric field is easy to access as demonstrated experimentally in our work. Note that the duration of the electric field would be extremely short (100 ns). Therefore, it would not change the local polarization axis as in the experiments shown in Fig. 2.

We now discuss the feasibility of generating a superposition of eigenstates with a resonant high-frequency electric field. An oscillating electric field at the frequency of f_E leads to a time dependent anisotropy $D(t) = D(E = 0) + \kappa E\cos(2\pi ft)$. This time-dependent $D(t)\ \hat{S}_z^2$ term can excite a spin transition when the resonance condition, $f_E = f_{34}$, is fulfilled. The Rabi rate of this electric field–driven transition is given by

$$f_{Rabi} = |\kappa E\langle m_s = -3/2\ |\hat{S}_z^2|\ m_s = +3/2\rangle| \quad (2)$$

where $|\ m_s = -3/2\rangle$ and $|\ m_s = +3/2\rangle$ correspond to the wave functions for the states.

Figure S5B shows the transition rate in Eq. 2 as a function of the angle between the H field and the c axis at 8000 Oe. A maximum Rabi rate of $f_{Rabi} = 0.194\kappa E = 1.94\ Hz\ V^{-1}\ m$ is found when the field is applied 70° away from the c axis. This implies that an oscillating electric field of 50 kV/cm would give rise to a Rabi frequency of 10 MHz, already 100 times faster than the decoherence rate of the −3/2 ↔ +3/2 EPR transition.

SUPPLEMENTARY MATERIALS

Supplementary material for this article is available at http://advances.sciencemag.org/cgi/content/full/7/10/eabf8103/DC1

REFERENCES AND NOTES

1. S. Manipatruni, D. E. Nikonov, C.-C. Lin, T. A. Gosavi, H. Liu, B. Prasad, Y.-L. Huang, E. Bonturim, R. Ramesh, I. A. Young, Scalable energy-efficient magnetoelectric spin–orbit logic. *Nature* **565**, 35–42 (2019).
2. S. Dong, J. -M. Liu, S. -W. Cheong, Z. Ren, Multiferroic materials and magnetoelectric physics: Symmetry, entanglement, excitation, and topology. *Adv. Phys.* **64**, 519–626 (2015).

3. C. Song, B. Cui, F. Li, X. Zhou, F. Pan, Recent progress in voltage control of magnetism: Materials, mechanisms, and performance. *Prog. Mater. Sci.* **87**, 33–82 (2017).
4. W. Huang, Y. Yin, X. Li, Atomic-scale mapping of interface reconstructions in multiferroic heterostructures. *Appl. Phys. Rev.* **5**, 041110 (2018).
5. H. Ohno, A window on the future of spintronics. *Nat. Mater.* **9**, 952–954 (2010).
6. V. Garcia, M. Bibes, L. Bocher, S. Valencia, F. Kronast, A. Crassous, X. Moya, S. Enouz-Vedrenne, A. Gloter, D. Imhoff, C. Deranlot, N. D. Mathur, S. Fusil, K. Bouzehouane, A. Barthelemy, Ferroelectric control of spin polarization. *Science* **327**, 1106–1110 (2010).
7. B. E. Kane, A silicon-based nuclear spin quantum computer. *Nature* **393**, 133–137 (1998).
8. J. J. Pla, K. Y. Tan, J. P. Dehollain, W. H. Lim, J. J. L. Morton, D. N. Jamieson, A. S. Dzurak, A. Morello, A single-atom electron spin qubit in silicon. *Nature* **489**, 541–545 (2012).
9. S. H. Chun, Y. S. Chai, B. G. Jeon, H. J. Kim, Y. S. Oh, I. Kim, H. Kim, B. J. Jeon, S. Y. Haam, J. Y. Park, S. H. Lee, J. H. Chung, J. H. Park, K. H. Kim, Electric field control of nonvolatile four-state magnetization at room temperature. *Phys. Rev. Lett.* **108**, 177201 (2012).
10. S. Valencia, A. Crassous, L. Bocher, V. Garcia, X. Moya, R. O. Cherifi, C. Deranlot, K. Bouzehouane, S. Fusil, A. Zobelli, A. Gloter, N. D. Mathur, A. Gaupp, R. Abrudan, F. Radu, A. Barthélémy, M. Bibes, Interface-induced room-temperature multiferroicity in $BaTiO_3$. *Nat. Mater.* **10**, 753–758 (2011).
11. D. Chiba, S. Fukami, K. Shimamura, N. Ishiwata, K. Kobayashi, T. Ono, Electrical control of the ferromagnetic phase transition in cobalt at room temperature. *Nat. Mater.* **10**, 853–856 (2011).
12. R. O. Cherifi, V. Ivanovskaya, L. C. Phillips, A. Zobelli, I. C. Infante, E. Jacquet, V. Garcia, S. Fusil, P. R. Briddon, N. Guiblin, A. Mougin, A. A. Unal, F. Kronast, S. Valencia, B. Dkhil, A. Barthelemy, M. Bibes, Electric-field control of magnetic order above room temperature. *Nat. Mater.* **13**, 345–351 (2014).
13. C. G. Duan, J. P. Velev, R. F. Sabirianov, Z. Zhu, J. Chu, S. S. Jaswal, E. Y. Tsymbal, Surface magnetoelectric effect in ferromagnetic metal films. *Phys. Rev. Lett.* **101**, 137201 (2008).
14. S. W. Yang, R. C. Peng, T. Jiang, Y. K. Liu, L. Feng, J. J. Wang, L. Q. Chen, X. G. Li, C. W. Nan, Non-volatile 180° magnetization reversal by an electric field in multiferroic heterostructures. *Adv. Mater.* **26**, 7091–7095 (2014).
15. M. Gejek, M. Bibes, S. Fusil, K. Bouzehouane, J. Fontcuberta, A. Barthélémy, A. Fert, Tunnel junctions with multiferroic barriers. *Nat. Mater.* **6**, 296–302 (2007).
16. A. V. Sadovnikov, A. A. Grachev, E. N. Beginin, S. E. Sheshukova, Y. P. Sharaevskii, S. A. Nikitov, Voltage-controlled spin-wave coupling in adjacent ferromagnetic-ferroelectric heterostructures. *Phys. Rev. Applied* **7**, 014013 (2017).
17. J. T. Heron, J. L. Bosse, Q. He, Y. Gao, M. Trassin, L. Ye, J. D. Clarkson, C. Wang, J. Liu, S. Salahuddin, D. C. Ralph, D. G. Schlom, J. Iniguez, B. D. Huey, R. Ramesh, Deterministic switching of ferromagnetism at room temperature using an electric field. *Nature* **516**, 370–373 (2014).
18. T. Maruyama, Y. Shiota, T. Nozaki, K. Ohta, N. Toda, M. Mizuguchi, A. A. Tulapurkar, T. Shinjo, M. Shiraishi, S. Mizukami, Y. Ando, Y. Suzuki, Large voltage-induced magnetic anisotropy change in a few atomic layers of iron. *Nat. Nanotechnol.* **4**, 158–161 (2009).
19. M. Fechner, P. Zahn, S. Ostanin, M. Bibes, I. Mertig, Switching magnetization by 180° with an electric field. *Phys. Rev. Lett.* **108**, 197206 (2012).
20. R. Hanson, D. D. Awschalom, Coherent manipulation of single spins in semiconductors. *Nature* **453**, 1043–1049 (2008).
21. A. K. Boudalis, J. Robert, P. Turek, First demonstration of magnetoelectric coupling in a polynuclear molecular nanomagnet: Single-crystal EPR studies of $[Fe_3O(O_2CPh)_6(py)_3]ClO_4$ py under static electric fields. *Chemistry* **24**, 14896–14900 (2018).
22. J. Liu, J. Mrozek, W. K. Myers, G. A. Timco, R. E. P. Winpenny, B. Kintzel, W. Plass, A. Ardavan, Electric field control of spins in molecular magnets. *Phys. Rev. Lett.* **122**, 037202 (2019).
23. M. Fittipaldi, A. Cini, G. Annino, A. Vindigni, A. Caneschi, R. Sessoli, Electric field modulation of magnetic exchange in molecular helices. *Nat. Mater.* **18**, 329–334 (2019).
24. J. van Slageren, Spin-electric coupling. *Nat. Mater.* **18**, 300–301 (2019).
25. W. L. Warren, G. E. Pike, K. Vanheusden, D. Dimos, B. A. Tuttle, J. Robertson, Defect-dipole alignment and tetragonal strain in ferroelectrics. *J. Appl. Phys.* **79**, 9250–9257 (1996).
26. K. A. Muller, W. Berlinger, Microscopic probing of order-disorder versus displacive behavior in $BaTiO_3$ by Fe^{3+} EPR. *Phys. Rev. B* **34**, 6130–6136 (1986).
27. V. V. Laguta, M. D. Glinchuk, I. P. Bykov, Y. L. Maksimenko, J. Rosa, L. Jastrabík, Impurity centers in $PbTiO_3$ single crystals: An electron-spin-resonance analysis. *Phys. Rev. B* **54**, 12353–12360 (1996).
28. D. J. Keeble, M. Loyo-Menoyo, Z. I. Y. Booq, R. R. Garipov, V. V. Eremkin, V. Smotrakov, Fe^{3+} defect dipole centers in ferroelectric $PbTiO_3$ studied using electron paramagnetic resonance. *Phys. Rev. B* **80**, 014101 (2009).
29. T. von Waldkirch, K. A. Müller, W. Berlinger, Analysis of the Fe^{3+}-V_O center in the tetragonal phase of $SrTiO_3$. *Phys. Rev. B* **5**, 4324–4334 (1972).
30. J. M. Zadrozny, J. Niklas, O. G. Poluektov, D. E. Freedman, Millisecond coherence time in a tunable molecular electronic spin qubit. *ACS Cent. Sci.* **1**, 488–492 (2015).
31. W. D. Oliver, P. B. Welander, Materials in superconducting quantum bits. *MRS Bulletin* **38**, 816–825 (2013).
32. W. B. Mims, *The Linear Electric Field Effect in Paramagnetic Resonance* (Oxford Univ. Press, 1976).
33. R. E. George, J. P. Edwards, A. Ardavan, Coherent spin control by electrical manipulation of the magnetic anisotropy. *Phys. Rev. Lett.* **110**, 027601 (2013).
34. F. R. Bradbury, A. M. Tyryshkin, G. Sabouret, J. Bokor, T. Schenkel, S. A. Lyon, Stark tuning of donor electron spins in silicon. *Phys. Rev. Lett.* **97**, 176404 (2006).
35. S. C. Benjamin, Schemes for parallel quantum computation without local control of qubits. *Phys. Rev. A* **61**, 020301 (2000).
36. S. C. Benjamin, S. Bose, Quantum computing with an always-on heisenberg interaction. *Phys. Rev. Lett.* **90**, 247901 (2003).
37. M. E. Lines, A. M. Glass, *Principles and Applications of Ferroelectrics and Related Materials* (Oxford Univ. Press, 1977).
38. G. Kresse, J. Hafner, *Ab initio* molecular-dynamics simulation of the liquid-metal–amorphous-semiconductor transition in germanium. *Phys. Rev. B* **49**, 14251–14269 (1994).
39. G. Kresse, J. Furthmüller, Efficiency of ab-initio total energy calculations for metals and semiconductors using a plane-wave basis set. *Comput. Mater. Sci.* **6**, 15–50 (1996).
40. G. Kresse, J. Furthmüller, Efficient iterative schemes for *ab initio* total-energy calculations using a plane-wave basis set. *Phys. Rev. B* **54**, 11169–11186 (1996).
41. P. E. Blöchl, Projector augmented-wave method. *Phys. Rev. B* **50**, 17953–17979 (1994).
42. G. Kresse, D. Joubert, From ultrasoft pseudopotentials to the projector augmented-wave method. *Phys. Rev. B* **59**, 1758–1775 (1999).
43. S. L. Dudarev, G. A. Botton, S. Y. Savrasov, C. J. Humphreys, A. P. Sutton, Electron-energy-loss spectra and the structural stability of nickel oxide: An LSDA+U study. *Phys. Rev. B* **57**, 1505–1509 (1998).
44. E. L. Hahn, Spin echoes. *Phys. Rev.* **80**, 580–594 (1950).
45. J. Kobajashi, S. Okamoto, R. Ueda, Dielectric behavior of lead titanate at low temperature. *Phys. Rev.* **103**, 830–831 (1956).

Acknowledgments

Funding: The work at UC Berkeley was supported in part by the Center for Probabilistic Spin Logic for Low-Energy Boolean and Non-Boolean Computing (CAPSL), one of the Nanoelectronic Computing Research (nCORE) Centers as task 2759.002, and a Semiconductor Research Corporation (SRC) program sponsored by the NSF through CCF 1739635. Partial support from the U.S. Department of Energy (DOE) EFRC on Quantum Coherence is acknowledged. The materials theory/calculation work (to K.I. and S.M.G.) was supported by the Laboratory Directed Research and Development Program of Lawrence Berkeley National Laboratory under DOE contract no. DE-AC02-05CH11231. E.S. acknowledges support from the U.S.-Irish Fulbright Commission and work supported by the Air Force Office of Scientific Research under award number FA9550-18-1-0480. Computational resources were provided by the National Energy Research Scientific Computing Center and the Molecular Foundry, DOE Office of Science User Facilities supported by the Office of Science, DOE under contract no. DE-AC02-05CH11231. The work performed at the Molecular Foundry was supported by the Office of Science, Office of Basic Energy Sciences, of the DOE under the same contract. V.V.L. thanks the support from the Ministry of Education, Youth, and Sports of Czech Republic under project no. SOLID21-CZ.02.1.01/0.0/0.0/16_019/0000760. A.A. acknowledges support from the Engineering and Physical Sciences Research Council (EP/P000479/1), the QuantERA European Project SUMO, and the European Union's Horizon 2020 research and innovation program under grant agreement numbers 863098 (SPRING) and 862893 (FATMOLS). R.C. thanks the Division of Chemical Sciences, Geosciences, and Biosciences of the DOE (contract no. DE-AC02-05CH11231). **Author contributions:** R.R., A.A., V.V.L., S.M.G., S.D., and W.H. designed the experiments. J.L. and V.V.L. performed EPR and spin echo measurement for the single crystals, along with the detailed analyses. K.I., E.S., and S.M.G. performed DFT calculations. R.R., S.M.G., W.H., J.L., S.D., K.I., A.A., and V.V.L. analyzed the data and cowrote the manuscript. R.R., S.M.G., and A.A. supervised the research. All authors contributed to the discussions and manuscript preparation. **Competing interests:** The authors declare that they have no competing interests. **Data and materials availability:** All data needed to evaluate the conclusions in the paper are present in the paper and/or the Supplementary Materials. Additional data related to this paper may be requested from the authors.

Submitted 22 November 2020
Accepted 19 January 2021
Published 3 March 2021
10.1126/sciadv.abf8103

Citation: J. Liu, V. V. Laguta, K. Inzani, W. Huang, S. Das, R. Chatterjee, E. Sheridan, S. M. Griffin, A. Ardavan, R. Ramesh, Coherent electric field manipulation of Fe^{3+} spins in $PbTiO_3$. *Sci. Adv.* **7**, eabf8103 (2021).

Science Advances

Coherent electric field manipulation of Fe^{3+} spins in $PbTiO_3$

Junjie Liu, Valentin V. Laguta, Katherine Inzani, Weichuan Huang, Sujit Das, Ruchira Chatterjee, Evan Sheridan, Sinéad M. Griffin, Arzhang Ardavan and Ramamoorthy Ramesh

Sci Adv **7** (10), eabf8103.
DOI: 10.1126/sciadv.abf8103